Evaluation of SuperMAG auroral electrojet indices as indicators of substorms and auroral power

P. T. Newell[1] and J. W. Gjerloev[1]

Received 22 April 2011; revised 19 September 2011; accepted 24 September 2011; published 14 December 2011.

[1] We use magnetometer chains collaborating with SuperMAG to derive *SME*, a generalization of the auroral electrojet indices calculated from 100 or more sites instead of the 12 used in the official auroral electrojet indices, $AE(12) = AU(12) - AL(12)$. We investigate how these various indices relate to nightside auroral power by using both particle (DMSP) and image (Polar Ultraviolet Imager (UVI)) data. The best correlation is between *SME* and total nightside auroral power, namely, $r = 0.86$. Hence, nearly 3/4 of the minute-by-minute variance in nightside power can be determined by *SME* alone. Interestingly, although the geophysical meaning of *AE*(12) has sometimes been challenged, we show that even that index correlates at the $r = 0.81$ level, or 2/3 of the variance, in nightside power. Most auroral power stems from the diffuse aurora, with a linear relationship between the auroral electrojet indices and nightside diffuse power. Thus, *SME* has a clear geophysical meaning: It samples the thermal portion of the magnetotail plasma sheet. We study how well *SML* (the generalization of *AL*) identifies substorms in two types of tests. The first is a comparison with a set of 1081 substorms determined from Polar UVI in 1997–1998, and the second is the use of DMSP particle precipitation data for superposed epoch analysis. The same algorithm applied to *SML* is much more likely (about 50% more likely) to identify an onset seen by UVI than is *AL*(12). Even when both indices can be used to identify onsets, the median delay after imaging onset until the *AL* indicator is less than half using *SML* (about 4 min versus 8 min). There are 10,719 onsets in the *SML* data between 1 January 1997 and 31 December 2002, of which 5084 are isolated. Isolated *SML* onsets behave almost identically to the onsets determined by global imagers. Specifically, they represent the same sharp spike in auroral power, which is most pronounced in broadband (wave) precipitation, with the same duration and subsequent recovery. However, recurrent substorms (those following less than 2 h after a previous onset) rise from a higher baseline by a smaller percentage but with the same absolute change in auroral power, thus reaching a higher peak power.

Citation: Newell, P. T., and J. W. Gjerloev (2011), Evaluation of SuperMAG auroral electrojet indices as indicators of substorms and auroral power, *J. Geophys. Res.*, *116*, A12211, doi:10.1029/2011JA016779.

1. Introduction

[2] No alternative characterizes magnetospheric activity on a global scale with the same continuity and high time resolution as an appropriately selected magnetic index. Substorms are a perennially favorite topic for magnetospheric researchers, and *AL* appears to be the index which best corresponds to substorm activity. Prior to onset, *AL* is typically small in magnitude, with the contributing station near dawn, whereas after onset the contributing station lies under the auroral onset bulge [*Gjerloev et al.*, 2004]. The magnitude of *AL* is a good indicator of the strength of a substorm. And yet its usage has been severely constrained. Partly this is because of the slowness of distribution of high time resolution *AL* data (or even, at times, limited distribution). But it is widely suspected that there may be uncertainties which arise from the limited number of geomagnetic stations (12) involved in creating the traditional indices [e.g., *Rostoker*, 1972; *Davis and Sugiura*, 1966; *Ahn et al.*, 2000]. We will here call the traditionally derived index Auroral Electrojet indices $AE(12) = AU(12) - AL(12)$, where *AU* and *AL* are the upper and lower components of *AE* (the largest and smallest values of the *H* component among the magnetic stations used).

[3] Here we investigate whether the SuperMAG collaboration [*Gjerloev*, 2009] involving a large number of chains around the world can enhance the value of *AE* and *AL*. More generally, we wish to quantify the performance of *AL* as a substorm indicator, and of *AE* as a predictor of gross nightside auroral activity. The number of stations contributing to this enhanced variant of *AE* varies between 83 and 120, but

[1]Johns Hopkins University Applied Physics Laboratory, Laurel, Maryland, USA.

0148-0227/11/2011JA016779

Table 1. Magnetometer Chains or Collaborative Efforts Contributing to SuperMAG

Magnetometer Chain	Principal Investigator (or contributor to SuperMAG)
Intermagnet	J. J. Love, D. Boteler, A. Chulliat, D. Kerridge
AUTUMN	M. Connors
CARISMA	I. Mann
CANMOS	D. Boteler
210 Chain	K. Yumoto
AARI Chain	O. Troshichev
BGS Magnetometers	S. McMillan
MACCS Program	M. Engebretson and J. Hughes
MEASURE	M Moldwin and UCLA/IGPP
S-RAMP	K. Yumoto and K. Shiokawa
SAMNET	F. Honary
SPIDR	NOAA/NGDC
SAMBA[a]	E. Zesta
IMAGE	IMAGE team (10 institutes), E. Tanskanen
IZMIRAN magnetometers[a]	V. Kuznetsov and V. Petrov
Greenland magnetometers	DTU Space, C. Stolle
PENGUIn,[a] ICESTAR	L. J. Lanzerotti, A. T. Weatherwax
McMac	P. Chi

[a]Chains not currently used in the construction of the *SME* index.

is typically more than 100. Conceptually, the new index is simply *AE*(100), that is, *AE* evaluated using a large number of stations. However, since *AE* is an official and well established index with endorsement from IAGA, we avoid confusion by terming the new index *SME* (SuperMAG electrojet index). The questions posed above have clear answers. First, *SME* proves to be intimately related to precipitating auroral power on the nightside. In fact, it is possible to predict nearly 3/4 of the variance in nightside power at a 1 min cadence using *SME*. Similarly, it is possible to identify far more substorms, and to time them better with *SML* than with *AL*(12). We also introduce a technique by which substorm onset identification techniques can be quantitatively tested, at least for a large ensemble (a few thousand onsets or more).

2. Background and Data Sets

2.1. The SuperMAG Initiative

[4] SuperMAG is a worldwide collaboration of organizations and national agencies that currently operate ~300 ground-based magnetometers. A list of the contributors can be found in Table 1 (the footnoted entries are not currently incorporated in the construction of the *SME* index). SuperMAG utilizes vector measurements of the magnetic field, which represent a variety of file formats, temporal resolutions, units, and coordinate systems, and are provided with or without baseline subtracted. SuperMAG resamples the data to 1 min temporal resolution and converts all units into nanoteslas (nT). Artifacts and errors are removed or corrected by automated as well as manual correction routines. Data are then rotated into a local geomagnetic coordinate system, and finally the baseline is determined and subtracted by an automated objective technique. Studies of the variations caused by electric currents flowing in the ionosphere and magnetosphere require a subtraction of the dominant and slowly varying Earth main field. Hence, both absolute and variometer data (data with unknown baselines) are included in SuperMAG. The *SME* index, and a processed version of some other data, along with further information are available at the site supermag.jhuapl.edu. Those wishing original data are urged to contact the responsible principal investigators for the actual individual chains.

2.2. Definition of *AL*, *AU*, and *AE*: Extension to *SME*

[5] The auroral electrojet indices *AL* and *AU* have been used extensively since they were first introduced by *Davis and Sugiura* [1966]. Historically the indices have been used as an indicator of auroral electrojet activity and thereby the magnetospheric activity. The auroral electrojet indices are scalar values, which indicate the maximum perturbation measured at one of the *AE* station locations. Hence, they are local indices, and measure global electrojet activity only to the extent that station coverage is global. The current *AE* network consists of 12 stations strategically placed around the globe to minimize these limitations. In this paper we will show that even *AE*(12) is more closely related to auroral power than previously suspected.

[6] Due to the popularity of *AU/AL* their limitations have been discussed, including UT and seasonal effects [*Rostoker*, 1972; *Allen and Kroehl*, 1975; *Ahn et al.*, 2000, 2002]. The main limitation is due to the small number of magnetometer stations used (10–12 stations) and their uneven spatial distribution (see Figure 1) thereby implying that large auroral events can go undetected. This problem was realized even by *Davis and Sugiura* [1966]. *AE* stations have wide local time gaps (average of 2 h and up to 3.2 h between Tixie Bay and Cape Wellen), which are potentially inadequate. This led *Rostoker* [1972] to conclude that the index should be used only in statistical studies rather than individual events. The use of a larger number of stations to derive *AE* has been previously explored for a limited number of days [*Kamide et al.*, 1982], although the performance advantage over the traditional index was not investigated.

[7] The *SME* index introduced here differs from the traditional *AE* index primarily by the number of stations sampled. All data are first transformed into coordinates with the *H* component pointing toward local magnetic north. The baseline is subtracted according to the following paragraph. Then the station with the largest *H* value contributes the *SMU* value, while the station with the smallest value contributes *SML*. *SME* is the difference between the envelopes, $SME = SMU - SML$.

[8] Determining the baseline is a fundamental problem with no single right method. Historically, baselines for a given day have been removed by manually identifying a nearby quiet day, which then is taken to be the baseline. The data volume for the SuperMAG collaboration does not permit this method. The SuperMAG initiative requires an automated and objective baseline method, since decades of data from more than 300 stations are included. One of us (JWG) therefore developed a new automated procedure for determination of the undisturbed daily variations of the magnetic field [*Hoffman and Gjerloev*, 2008], which forms the baseline. The automated procedure removes the yearly trend as well as daily variation (including contributions from the *Sq* current system) in two separate steps: (1) a determination of the yearly trend and (2) a determination of the daily variations. Both steps use a sliding window and bin data according to magnitude, and determine a typical value. For example, the yearly trend is calculated by determining a

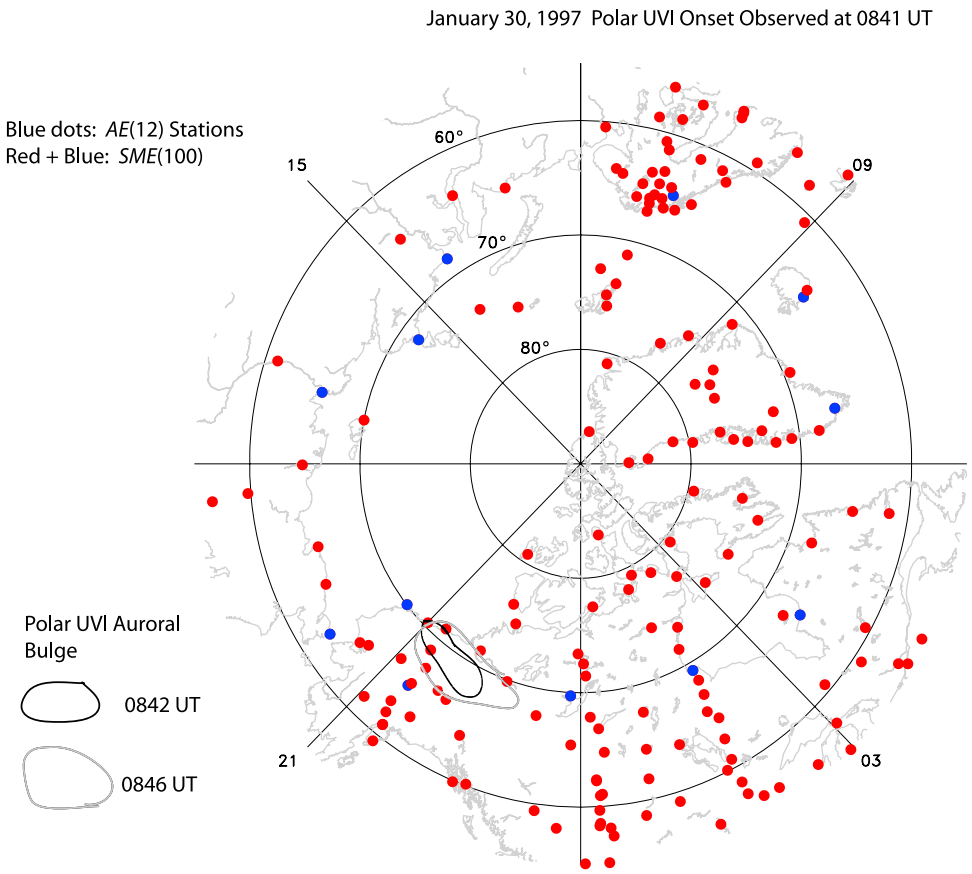

Figure 1. The geomagnetic stations used for *AL*(12) and for *SML*(100), with the ionosphere appropriate to 30 January 1997 at 0841 UT, when a substorm onset was observed by Polar UVI. The location of the onset auroral bulge is drawn for two epochs. Note that no *AL*(12) stations lay beneath the onset bulge.

single value for each day which is then subtracted from the 1 min data after a simple interpolation between discrete daily values (since the change from one day to the next is typically <1 nT, no more complex interpolation is meaningful). This single value is determined for day *N* using a 17 day window centered at day *N*. The 17 day window was chosen to balance the competing interests of avoiding seasonal variations, which favors a shorter window, and avoiding ring current perturbation, which favors a longer window. The value for this day is then determined by fitting a Gaussian to the distribution of the binned data. This technique is used to avoid the inherent problems for mean, which is affected by extreme values, and for the median, which implicitly assumes a symmetric distribution.

2.3. DMSP Data

[9] Data from the SSJ/4 electrostatic analyzers on the DMSP series satellites (F12 through F15), and the SSJ/5 detector on F16 were used. The time period covered is from 30 March 1996 through 31 December 2007.

[10] The DMSP satellites are in Sun-synchronous nearly circular polar orbits at about 845 km altitude, with orbital inclinations of 98.7 degrees. The orbits of the DMSP satellites are such that the least covered regions are postnoon and especially postmidnight, except at high magnetic latitudes. The SSJ/4 and SSJ/5 instruments included on all these flights uses curved plate electrostatic analyzers to measure electrons and ions with one complete spectrum each obtained per second. The satellites are three-axis stabilized; and the SSJ/4 detector apertures always point toward local zenith. At the latitudes of interest in this paper, this means that only highly field-aligned particles well within the atmospheric loss cone are observed. The SSJ/5 averages particles over a 90° swath from zenith to the spacecraft ram direction (and thus is largely, but not entirely, within the loss cone).

2.4. Polar Ultraviolet Imager Substorm Onsets

[11] The Polar Ultraviolet Imager (UVI) is primarily in the Lyman-Birge-Hopfield (LBH) bands of N_2, stimulated by atmospheric secondaries, and thus responsive to primary precipitating electrons above a few hundred eV energy (and ions as well, although the energy flux of the latter is typically far smaller). The typical time resolution between images is typically 1 min. The onset itself can only be identified by following an auroral expansion over time. Hence, the procedure largely consists of stepping backward in time away from a clear global expansion to the last frame where it still can be identified.

[12] Although storms were not explicitly excluded, it is harder to identify a single substorm onset during a storm from auroral imagery. This is because the process of backtracking to the first brightening is much more practical if initial conditions are quiet.

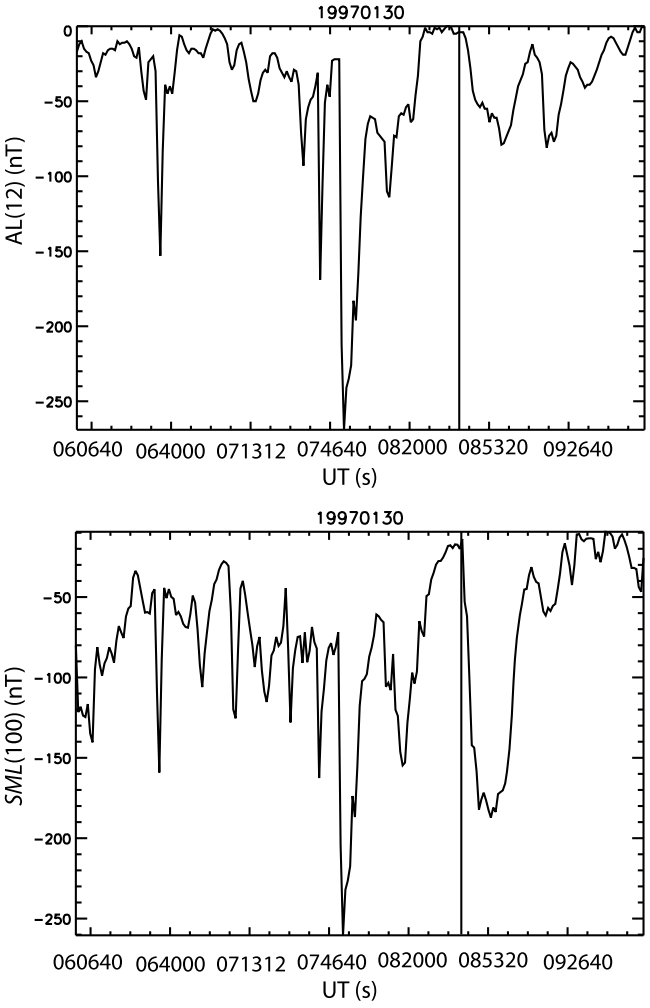

Figure 2. Following a series of brightenings and fadings, Polar UVI observed a sustained auroral breakup and expansion at 31,283 s of 30 January 1997 (vertical line). The substorm can be identified in the *SML*(100) data just 37 s later, while the traditional *AL*(12) does not pick up the actual onset.

[13] Polar UVI was equipped two filters to study the Lyman-Birge-Hopfield lines, one at shorter wavelengths (LBHS) and one longer (LBHL). Both filters are used, which improves time resolution. More information on the Polar UVI imager can be found in the works of *Liou et al.* [1997, 2001]. The substorm list used here is an extension by Dr. Kan Liou of the much smaller set of examples studied by *Liou et al.* [2001]. The same data set has been used in several previous papers [e.g., *Newell et al.*, 2010].

2.5. Superposed Epoch Techniques

[14] The procedure consists of analyzing every DMSP spectrum from 1 January 1996 through 31 December 2007, and classifying the precipitation as either monoenergetic, broadband, or diffuse aurora (in fact, that classification was previously performed for the work described by *Newell et al.* [2009]), and the resulting comprehensive list of classified spectra is used). Monoenergetic auroras are commonly called "inverted V" events, although in fact there are small potential gradients internally with large gradients typically on the edge [*Newell*, 2000]. Broadband aurora has long been associated with dispersive Alfvén wave acceleration, which has been better established in recent years [*Stasiewicz et al.*, 2000; *Chaston et al.*, 2003, 2004]. We believe that the close correspondence between broadband precipitating auroral power as surveyed by *Newell et al.* [2009], and the Poynting flux inflow to the ionosphere, as surveyed by *Chaston et al.* [2007], further establishes the connection.

[15] The epoch of each spectral observation (at 1 s cadence) is compared with the list of substorm onsets. If the particle observation is within 2 h of any onset it is added to the appropriate bin (determined from MLAT, MLT, and time from onset). It is possible for a single spectrum to be part of the "before" construction of a precipitation map based on one onset and "after" for another. In this case, it is added to both. Typically, a given satellite pass contributes to a variety of time step bins, since it takes about 25–30 min to cross the polar regions.

[16] The model resolution here is 48 MLT bins by 40 MLAT bins by 120 time step bins (the spatial resolution is reduced by a factor of 2 in both MLT and MLAT compared to our earlier work, reflecting the statistical limitations). The MLAT range is 50–90°, with data from the two hemispheres combined. Thus, although the identification of a substorm onset is based solely on northern hemisphere stations, the particle precipitation maps contain equal amounts of northern and southern hemisphere precipitation data, and thus represent the global variations in auroral power. The time step for precipitation map construction is 2 min, so that analysis begins 120 min before onset and extends to 120 min after.

[17] Hemispheric auroral power totals are computed by multiplying the physical surface area of each MLAT-MLT grid by the arithmetic energy flux mean to compute averages over the entire nightside. More details can be found in the work of *Newell et al.* [2010].

3. *AL*-Based Identification of Substorm Onsets

3.1. Case Example

[18] Figure 1 shows the distribution of the approximately 120 geomagnetic stations used in constructing *SME* and the 12 used in constructing the traditional *AE*(12). The geographic orientation shown is appropriate to 08:41 UT on 30 January 1997, which is also the time a substorm was identified by Polar UVI. This substorm is among the many hundreds for which movies have been created by Dr. Kan Liou of JHU/APL, and which are available at http://sd-www.jhuapl.edu/Aurora/polar_movies/UVI_polar_movies.html. Figure 1 also shows the location of the auroral breakup bulge at two epochs, namely, 08:42 UT and 08:46 UT. The bulge in this case expands eastward rather than westward (which, in fact, is quite often the case, despite the classic nomenclature of a "westward traveling surge"). The expansion of the auroral surge does not go over any of the *AE*(12) stations (blue dots), but does pass over more than a half dozen of the *SME* stations.

[19] Figure 2 shows the *AL*(12) and *SML* indices during a 4 h period including the onset time. A series of auroral brightenings and fadings occurred prior to onset, including a pseudo-onset at 07:53 UT. However, the onset time identified from the Polar UVI substorm database, namely 08:41 UT, is observed only be *SML*. It is clear that the absence of an

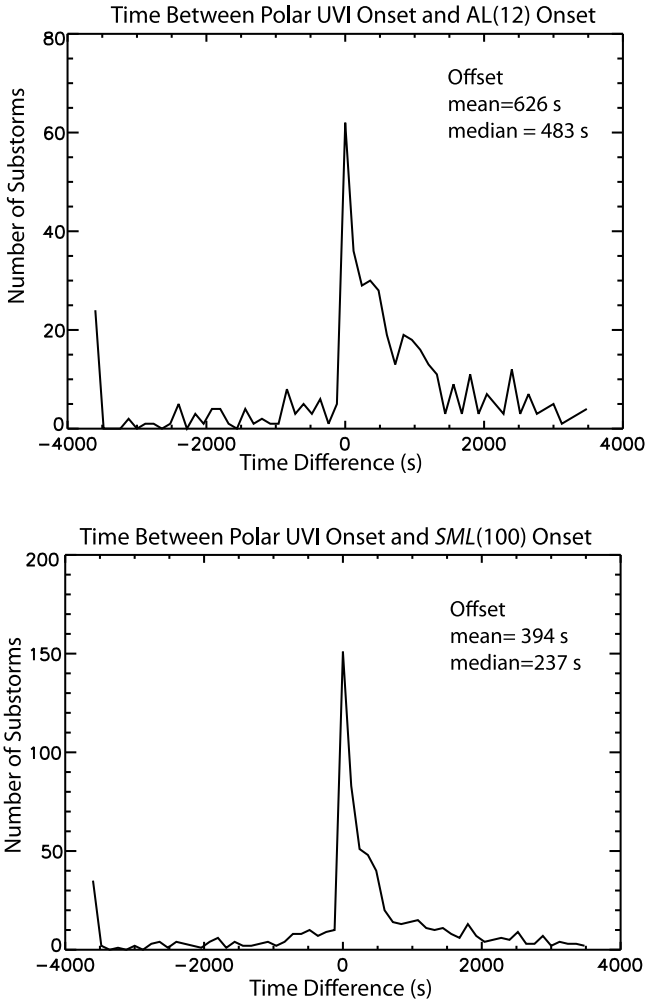

Figure 3. The time elapsed between Polar UVI observation of onset and identification by an AL algorithm for (top) *AL*(12) and (bottom) *SML*(100). The AL onset typically lags the UVI onset. The median delay is about twice as long for *AL*(12).

AL(12) station beneath the auroral bulge, as shown in Figure 1 results in virtually no detection of the sharp and sustained increase in auroral brightness at 08:41 UT. As discussed in section 2.3, the list of onset times from Polar UVI was established several years ago, are published on a public web site, and were not adjusted for this present work. Thus there is independent verification that, in this case at least, *AL*(12) does not perform nearly as well as *SML* is identifying substorms. The *AL*-based onset identification algorithm discussed in section 3.2 identified an onset 37 s after the Polar UVI determined onset using the *SML* data, but not at all using the *AL*(12) data.

3.2. *SML*-Based (or *AL*(12)-Based) Onset Identification Algorithm

[20] Based on previous experience with geophysical identification algorithms, we adopted a particularly simple set of criteria. When possible, this approach usually yields results that are more robust and have fewer unintended consequences than do more complex rules. The *SML* (and *AL*) data were considered at a 1 min cadence in a sliding 30 min buffer. An onset was identified at t_0 when four conditions are satisfied:

$$SML(t_0+1) - SML(t_0) < -15 \text{ nT} \quad (1)$$

$$SML(t_0+2) - SML(t_0) < -30 \text{ nT} \quad (2)$$

$$SML(t_0+3) - SML(t_0) < -45 \text{ nT} \quad (3)$$

$$\sum_{i=4}^{i=30} SML(t_0+\mathrm{i})/26 - SML(t_0) < -100 \text{ nT} \quad (4)$$

Thus the drop must be sharp (45 nT in 3 min), and sustained (must average 100 nT below the initial value for the remainder of the half hour). The *SML* onset is then placed at t_0, the last minute before a 15 nT drop. Once an onset is identified, the algorithm advances ahead 20 min, which is thus the minimum permitted time between two consecutive onsets. (In fact, only a relative handful of onsets do occur that close together.)

[21] The same algorithm was used for both *AL*(12) and *SML*. Nonetheless, more substorms are identified with *SML*. For 1997, the application of this algorithm to *AL*(12) data locates 1006 substorms onsets. For the same year and algorithm, 1397 onsets are found in the *SML* data (39% more). Similarly, for 1998, there are 1423 substorms identified in the *AL*(12) data, whereas there are 1856 onsets identified by the same algorithm in the *SML* data (30% more). These numbers are suggestive, but not definitive as to the improvement brought about by using *SML*. Therefore it is necessary to compare the two sets of onset identifications against other observations.

4. Onset Identification: Comparison With Polar UVI and DMSP

4.1. Comparison With Polar UVI

[22] The Polar UVI data set includes 2424 substorm onsets, individually identified by Dr. Kan Liou of JHU/APL. Of these, 1083 occur within the study interval, 1997–1998, all in the northern hemisphere. The timing of these onsets is intended to be accurate to about 30 s, and is listed to the nearest 1 s. The *AL* onset is taken to be the second which starts the 1 min interval meeting the criteria outlined in 3.1 (that is, the last minute prior to the first 15 nT drop). For each substorm, we calculated the time, Δt, between onset as observed by Polar UVI and by *AL*. This value can be either negative or positive. Perhaps unsurprisingly, the large majority of time Δt is positive, meaning that the *AL*-identified onset occurs after the Polar UVI onset. If no *AL* onset is located within 1 h of the Polar UVI onset, it is considered not to have identified the onset at all.

[23] Extending the time interval to 1 h allows us to verify that the coincidence rate trends rapidly toward a noise level. In fact, only a negligible number of coincident onsets were observed after 30 min, and those have a minuscule impact on the statistics provided (especially the calculated median delay, although the mean is a bit more affected).

[24] Figure 3 shows the distribution of Δt. A very sharp peak occurs at Δt = 0 (the 0–1 min bin), with a highly

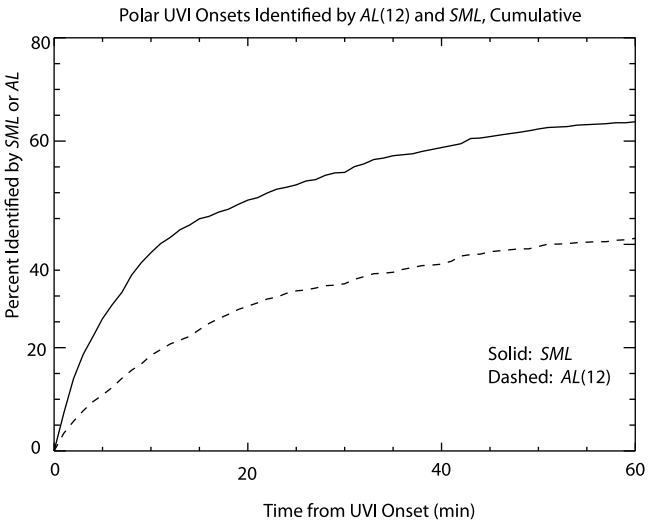

Figure 4. The fraction of Polar UVI onsets that also have an *SML*- or *AL*(12)-identified onset, as a cumulative function of time since UVI onset. *SML* is about 50% more likely to identify substorms than *AL*(12).

asymmetric distribution about 0. The *SML*-determined onset time is, in the great majority of cases, after the UVI-determined onset. The mean is well away from the peak, since there are a few cases that have up to 1 h delay (Δt larger than that are not counted). The median is perhaps the most reasonable comparison. For *AL*(12) the median is 483 s, whereas for *SML* the median is 237 s, or about half as long. Thus, for those cases where *AL* identifies a substorm around the Polar UVI identification, the time delay is much shorter using *SML*. A perpetual issue in substorm onset identification is distinguishing between the "real" onset and pseudo-onsets which precede the real one. That ambiguity exists whether looking at auroral images, in situ magnetotail data, or *AL* values. It is therefore possible, even likely, that in some instances, the AL onset time precedes the values chosen by Dr. Liou from Polar UVI, and yet the former is correct.

[25] As mentioned, in some cases there is no corresponding *AL* onset within 1 h of the UVI onset. Figure 4 shows the cumulative fraction of Polar UVI onsets identified from the two indices over the course of that hour, respectively. The *SML* index is much more likely to recognize the onset within the first few minutes. Even after 1 h, there is a greater than 50% higher identification of onsets with *SML* than with *AL*(12). One should not expect perfect agreement, since neither the Polar UVI instrument nor the determination of onsets from it is perfect. Indeed, there are not, even today, unambiguous and quantitative criteria for a substorm onset. Differences exist about the onset time even in well studied events by noted researchers using multiple instruments. We thus regard the fraction identified in Figure 4 as well below the fundamental accuracy of the *SML* approach.

4.2. DMSP-Based Comparison

[26] An auroral substorm, both as originally conceived and as generally regarded today, should represent a sharp increase in auroral power that persists for at least some tens of minutes. Here we use the superposed epoch analysis technique discussed in section 2.4 to investigate whether *SML* substorm onsets, as identified using the algorithm introduced here, meets those criteria. Unfortunately, to produce reasonable precipitation maps at a variety of time steps around onset appears to require many thousands of onsets. The nearly 5,000 onsets used by *Newell et al.* [2010] still left a few MLT/MLAT bins with only a few satellite passes (the bins used are already much wider than for constructing precipitation maps). As a result, we are only able to produce precipitation maps for *SML*, for which we have a total of 10,719 substorms spanning the years 1997–2002. (There are less than 2400 onsets for *AL*(12), all in 1996–1997, the only years for which we have 1 min AL data. There are only about 1000 isolated onsets, perhaps a quarter of the minimum needed for this type of analysis.)

[27] Figure 5 shows how two types of auroral precipitation vary around *SML* substorm onset. Figures 5a and 5b apply to diffuse electron precipitation (everything that is unaccelerated), and to broadband electron acceleration, using each of the 10,719 substorms. Monoenergetic aurora contributes significantly more power to the oval than does broadband acceleration, but we prefer to show broadband here because of its strong sensitivity to onset [*Newell et al.*, 2010]. The algorithms for identifying each type of aurora are detailed by *Newell et al.* [2009].

[28] Many of the substorms in the *SML* database are recurring, that is, occur shortly after a previous onset ("shortly" will be defined soon). There is strong interest in the community in isolated substorms, with some believing that an isolated onset differs from succeeding onsets. The term "isolated" is somewhat misleading, since it is almost always used to refer to an initial onset, regardless of whether any additional onsets follow. Nonetheless, adopting that terminology, we segregated our substorms into "isolated" onsets (those without any previous onsets in the preceding 2 h) and recurring onsets (those that follow within 2 h of a previous onset). In our data set, there are 5084 isolated onsets, and 5635 recurring onsets. Figures 5c and 5d show the behavior of the semihemispheric (nightside) power for the diffuse aurora and broadband aurora restricted to isolated onsets. For isolated onsets, the auroral power starts initially significantly lower, as might be expected. The jump in power is, however, higher when expressed as a percentage; for example, broadband aurora jumps by 186%, as opposed to the 84% rise seen when all onsets, including the recurring ones, are used. These figures for isolated substorms are very close to those reported by *Newell et al.* [2010] using the onset list of 4861 substorms identified by global imagers, consisting of 2424 onsets [*Liou et al.*, 2001] from Polar UVI and 2437 onsets from IMAGE [*Frey et al.*, 2004]. That study gave, for example, an 182% rise in auroral power for broadband aurora from the 2 h average before onset to the peak after onset. (At least one well-documented case study also demonstrated the connection between wave aurora and substorm onset: *Mende et al.* [2003].) In fact, there are no significant differences between the auroral power rise and fall of isolated substorms identified by *SML* and those identified by global images.

4.3. Isolated Versus Recurring Onsets

[29] One of the advantages of the use of geomagnetic indices to identify substorm onsets is the ability to do so continuously, under a wide variety of geomagnetic conditions.

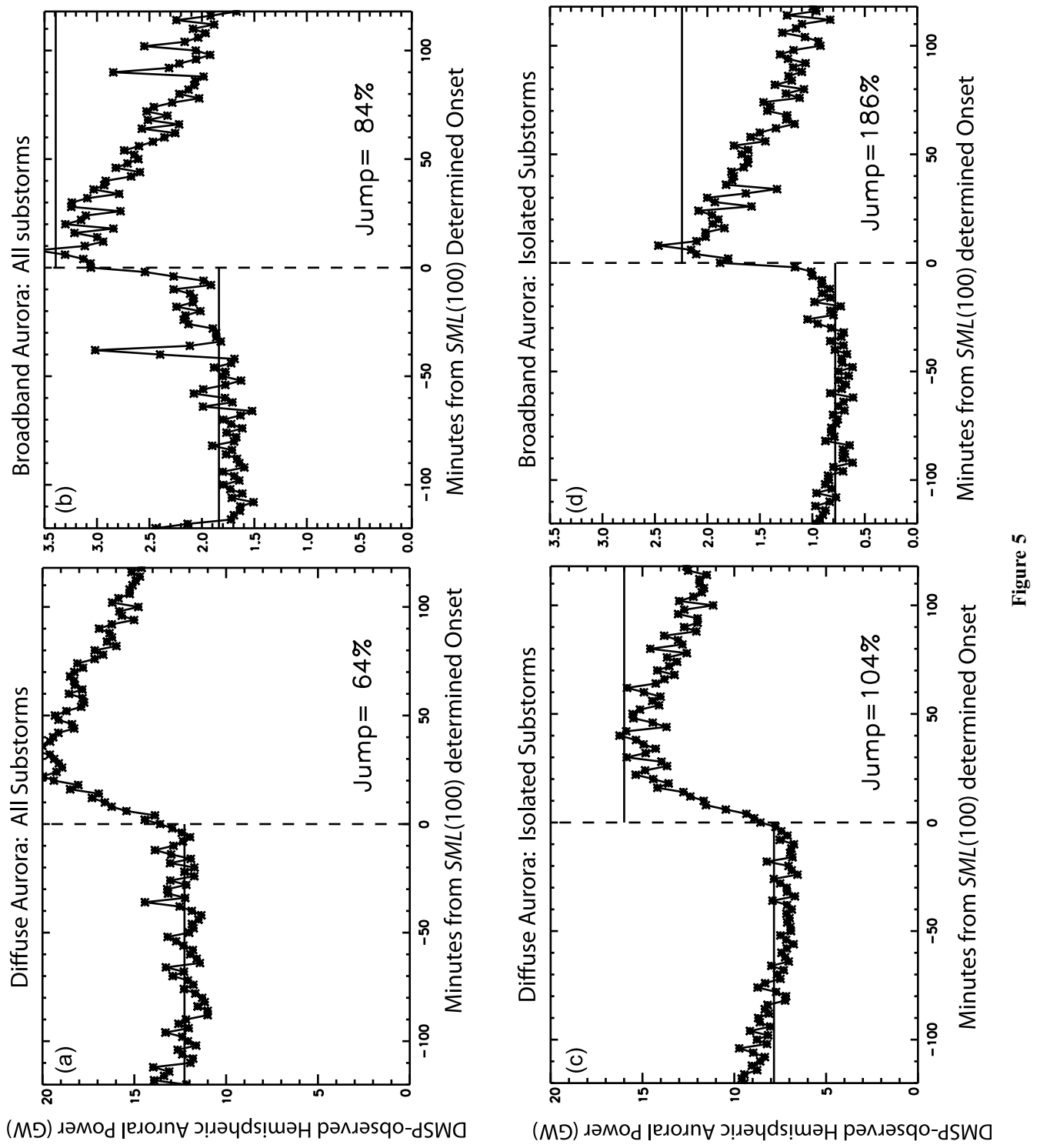
Diffuse Aurora: All Substorms
Broadband Aurora: All substorms
Diffuse Aurora: Isolated Substorms
Broadband Aurora: Isolated Substorms
(a)
(b)
(c)
(d)
Jump= 64%
Jump= 84%
Jump=104%
Jump=186%
DMSP-observed Hemispheric Auroral Power (GW)
Minutes from SML(100) determined Onset

Figure 5

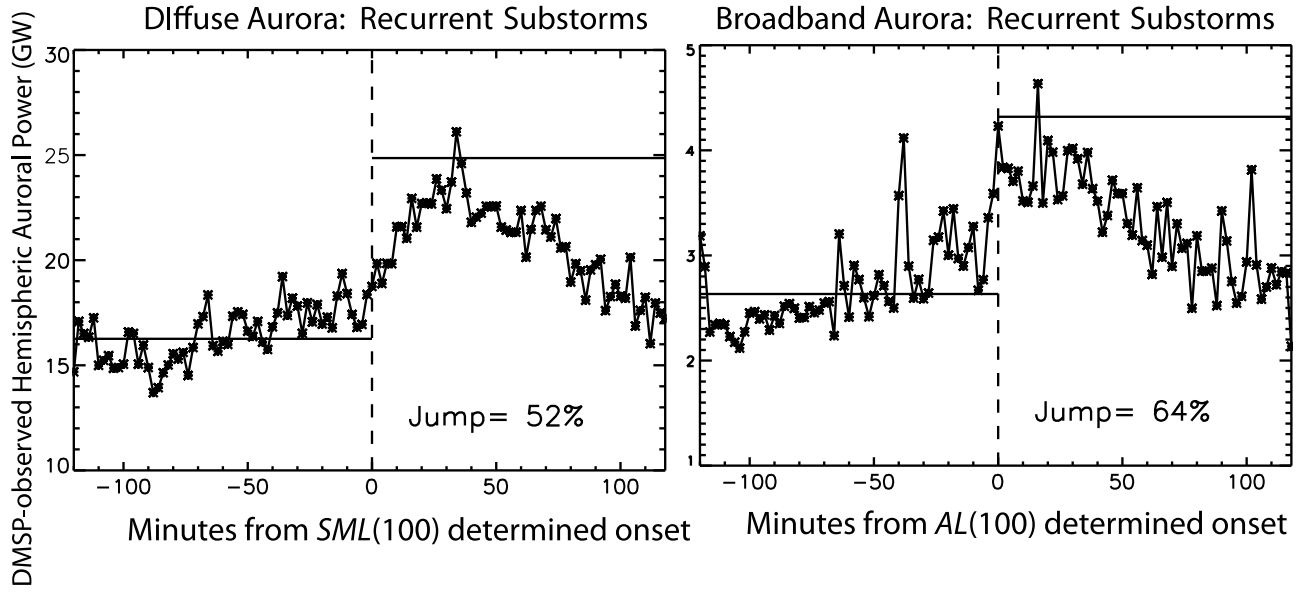

Figure 6. Nightside auroral power around substorm onset for the recurrent substorms in the *SML*(100) data. Recurrent substorms show much smaller relative increases in auroral power but, starting from a lower baseline, rise to a larger absolute value. Broadband precipitation in particular does not show the large relative gains seen for isolated onsets.

One way to illustrate this power is to contrast the results for recurrent versus isolated substorms. Figure 6 shows the diffuse and broadband auroral power for only recurrent substorms (those preceded by another onset over the previous 2 h). Figure 6 shows that recurrent substorms start from an appreciably higher baseline of auroral power. The diffuse aurora increases by "only" 52% as opposed to the 64% seen in isolated substorms. The difference in broadband (wave) aurora is far more striking, with just a 64% increase in precipitating power for recurrent substorms, versus the 186% increase seen for isolated substorms. In fact, for recurrent substorms, all three major types of electron precipitation increase on the order of 60%. By contrast, isolated substorms see a much sharper increase in broadband precipitation than in any other type. These findings do support the anecdotal perception that isolated substorms are different, and in some ways represent more of a dramatic change, than are any subsequent additional onsets.

[30] However (as was pointed out to us by one referee), unlike the relative power change, the absolute value of the change in auroral power is about the same for both isolated and recurrent substorms. Thus about a 8 GW rise is seen for diffuse aurora, and roughly 1.5 GW for broadband, whether isolated or recurrent substorms are considered. The larger percentage rise for isolated substorms is simply because of the start from a lower baseline.

5. *SME* Index and Auroral Power

[31] The most interesting result of the present paper is the close correlation between the *SME* index and auroral power, even when calculated at a 1 min cadence. Indeed, historically, the physical meaning and thus usefulness of *AE* has been questioned [*Kamide and Rostoker*, 2004]. It turns out that even *AE*(12) correlates much better with auroral power than other indices, including the ubiquitous *Kp*, or any known solar wind driving function. It is probably unsurprising that *SME* does even better, but it is surprising just how well total nightside auroral power can be predicted at a high time cadence. The geophysical meaning of the *SME* and *AE* indices are thus established.

5.1. Comparisons With Polar UVI

[32] Figure 7 shows how auroral power integrated over the nightside auroral oval from Polar UVI observations compares with *AE*(12) and *SME*. The integration covers 1800 MLT through 0600 MLT and 60° MLAT through 80° MLAT. Altogether there are 51,854 distinct 1 min images which cover both premidnight and postmidnight, nearly all at 1 min cadence, which were compared with *AE*(12) and *SME* over two years (1997 and 1998). In Figure 7, only 1 point out of 20 is plotted, but the correlation is with the full data set. *AE(*12) correlates with nightside auroral power at the r = 0.81 level, while *SME* correlates at the r = 0.86 level. Thus nearly 3/4 of all variance in integrated nightside auroral power can be predicted on the basis of *SME* alone, even at 1 min cadence.

[33] To appreciate how unusual this finding is, some points of comparison may help. IMF B_z correlates with nightside auroral power at $r = -0.51$, or about 1/4 of the variance (if it is suitably integrated over the previous 3 h), while *Kp* predicts at $r = 0.72$, or half the variance. Even at the 1 h cadence,

Figure 5. Semihemispheric (nightside) auroral power for 10,719 substorms identified by *SML*(100). Auroral power is computed as a composite from tens of thousands of DMSP satellite passes. (a) Diffuse aurora. (b) Broadband electron precipitation. (c, d) The same as Figures 5c and 5d, but the data are restricted to isolated substorms.

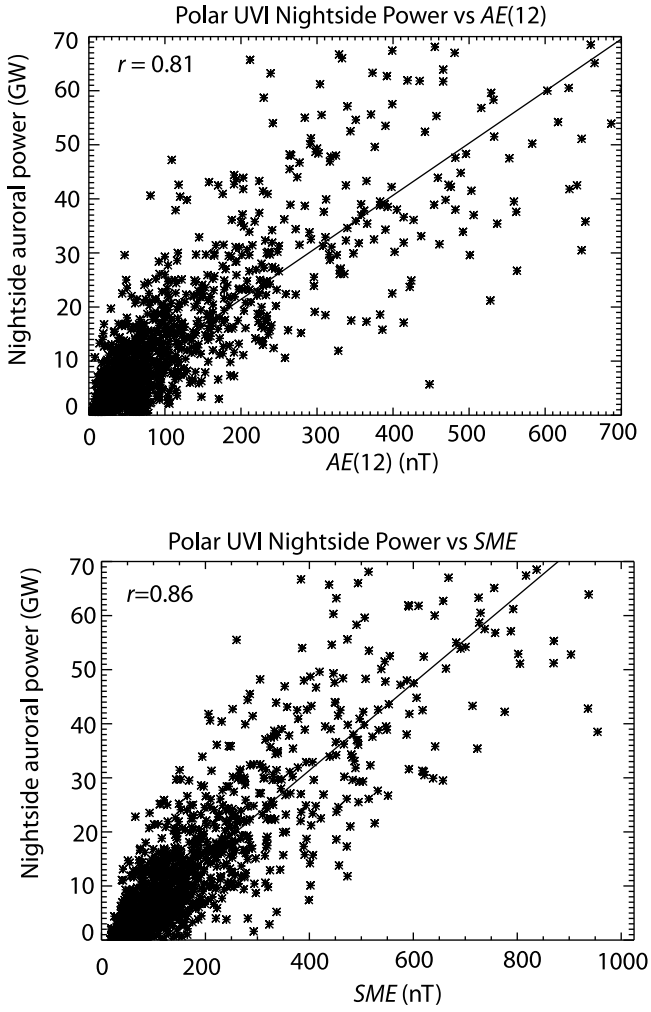

Figure 7. Scatterplots of nightside auroral power from Polar UVI versus *AE*(12) and *SME*. The tight correlation between auroral power and *AE*(12) is quite surprising, but the correlation with *SME* is even higher.

Kp does not do appreciably better, predicting less than half the variance in nightside auroral power. Out of scores of solar wind magnetosphere coupling functions tested, the best predictor of auroral power, namely, $d\Phi_{MP}/dt = v^{4/3}B_T^{2/3}\sin^{8/3}(\theta/2)$ (where $B_T = (B_y^2 + B_z^2)^{1/2}$, and θ is the IMF clock angle) [*Newell et al.*, 2007] only correlates at one minute cadence with r = 0.73 (still little more than half the variance).

[34] It might be wondered if premidnight auroral power better fits to *SMU* and postmidnight auroral power to *SML*, given that they typically represent the westward and eastward electrojet. We tried out each combination. Both premidnight and postmidnight auroral power correlates better with *SME* than with either component. For completeness, premidnight power (1800 to 0000 MLT, still integrated from 60° to 80° MLAT) correlates with *SMU*, *SML*, and *SME* at the level of r = 0.72, 0.77, and 0.84, respectively. Likewise, postmidnight (0000 through 0600 MLAT) auroral power correlates with *SMU*, *SML*, and *SME* at r = 0.73, 0.73, and 0.80 level.

[35] Thus the best correlation is between *SME* and total nightside power (which combines premidnight and postmidnight). The latter relationship is linear, at least to *SME* = 1200 nT. This can be seen in Figure 8, which groups the 51,854 individual images into bins. There is, however, an offset, with the Polar UVI observed power going to zero at *SME* = 50 nT. Because the imager does not respond to fluxes below about 0.25 erg/cm^2 s, and because quiet time auroral fluxes typically consist of low fluxes over broad areas, it seems likely that this is merely an artifact of instrument sensitivity. That is verified in section 5.2, which follows.

5.2. Auroral Power Comparisons With DMSP

[36] The DMSP data do not determine global auroral power on an instantaneous basis. However, DMSP data are sensitive to the 0.01 erg/cm^2 s level, and allow us to distinguish between the various types of aurora precipitation. Specifically, precipitation is separated into diffuse electron aurora, monoenergetic aurora ("inverted Vs"), broadband aurora (Alfvénic aurora), with ion precipitation also tracked. The algorithms for identifying each type have been previously specified in detail [*Newell et al.*, 2009, 2010] and will not be repeated here.

[37] We proceeded by constructing a series of precipitation maps in 5 nT bins of *SME*. The maps are standard

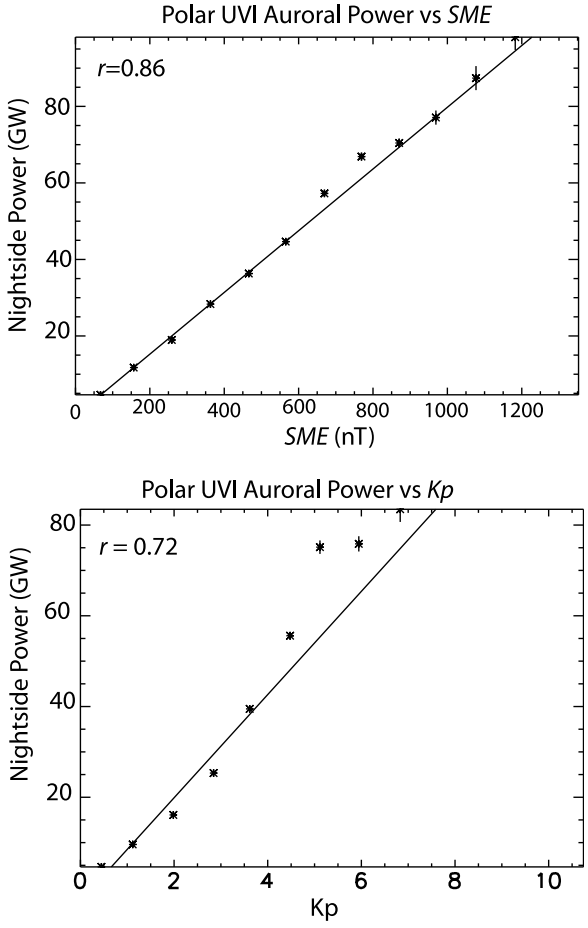

Figure 8. Polar UVI total nightside auroral power versus *SME* and *Kp*, collected into bins. The correlations listed are for the sample population, not the plotted means. Auroral power on the nightside is linear with *SME* but not with *Kp*.

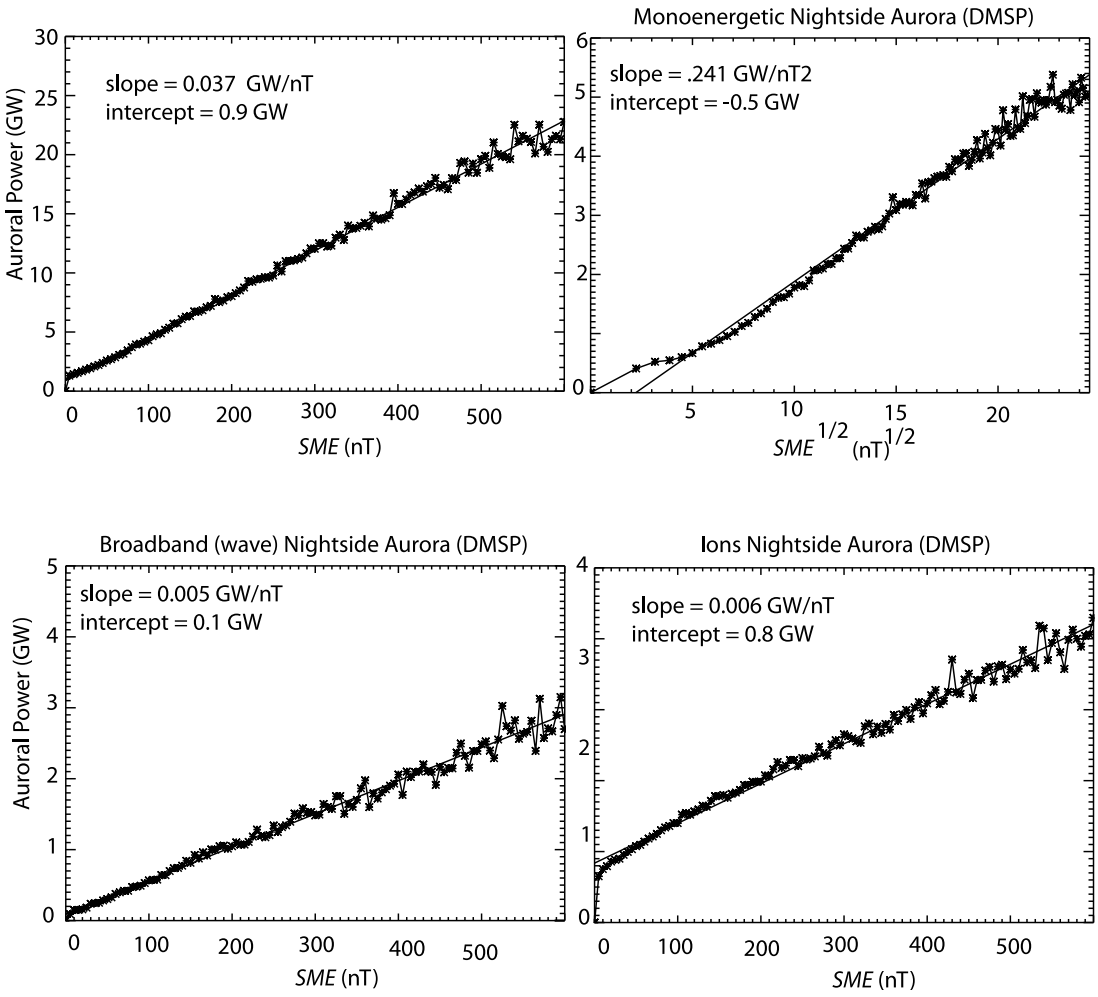

Figure 9. DMSP-based precipitation map values for each type of auroral precipitation. Auroral power is integrated over the nightside from 60 to 80 MLAT. Each asterisk (*) represents a single precipitation map for that value of *SME*. Monoenergetic aurora varies as the square root of *SME*; other types of aurora vary linearly with *SME*.

MLAT × MLT maps, using 11 years of DMSP data, 1996–2006. Each map is then integrated over the nightside auroral oval, from 60° to 80° MLAT and 1800–0600 MLT (the dayside does not part participate in substorms, and does not typically contribute to *SME*). Figure 9 shows the results of this approach for each type of aurora. One precipitation map, after integrating over the nightside oval, produces a single data point on Figure 9. First, note that based on the much more sensitive DMSP particle data, auroral precipitation does not go to zero for *SME* < 50 nT, as the Polar UVI imager data suggested. Instead, a small finite electron precipitation and slightly larger ion precipitation exists all the way down to the smallest bin, namely, *SME* = 0–5 nT.

[38] All types of auroral precipitation are linear with *SME*, except, interestingly, monoenergetic aurora, which varies as $SME^{1/2}$. Because we believe it may be generally useful, we reproduce here the relationships between auroral power and *SME*:

$$AP = 0.037*SME(\text{diffuse}) + 0.005*SME(\text{broadband}) + 0.006*SME(\text{ions}) + 0.241*SME^{1/2}(\text{monoenergetic}) \quad (5)$$

or, simplifying,

$$AP = 0.048*SME + 0.241(SME)^{1/2} \quad (6)$$

Here *AP* = nightside auroral power (integrated over 60–80° MLAT and 1800–0600 MLT). Some very modest offsets, amounting to a fraction of a GW globally, have been neglected in these equations. Since *SME* predicts about 3/4 of the minute-by-minute variance in nightside auroral power, these formulas provide a simple and direct way to estimate precipitation intensity for any epoch over the last three decades.

[39] It may be somewhat puzzling that monoenergetic aurora ramps more slowly with rising *SME* than do other types of aurora. In fact, monoenergetic aurora are quite common for relatively quiet and moderate times, all along the dusk to midnight oval, especially toward the poleward portion (indeed, the poleward edge of the oval here is typically demarcated by monoenergetic aurora). Precisely at substorm onset, both types of discrete aurora ramp up much faster than does diffuse aurora (this can be seen somewhat in Figure 5, but *Newell et al.* [2010] included more detail). However, discrete auroras quickly recover and fall back in 10–20 min,

whereas diffuse auroral power continues to ramp, maximizing 30–50 min after onset, and taking hours to decay. Thus on a gross scale, monoenergetic aurora represents a smaller portion of the total in the 2–3 h after a substorm than before. Of course on an absolute scale, there is more monoenergetic or inverted V aurora for more disturbed times. More specifically shortly after onset this type of aurora experiences a short-lived abrupt rise.

6. Summary and Conclusions

[40] We have established that a surprisingly clear geophysical meaning exists for *SME*: it represents the nightside integrated auroral power, which is dominated by diffuse aurora, to a surprising degree of accuracy. Specifically, even at a one minute cadence, *SME* correlates at $r = 0.86$ level with nightside auroral precipitating power, or about 3/4 of the variance. We also demonstrated that even the traditional *AE*(12) can predict about 2/3 of the variance ($r = 0.81$) at a one minute cadence. Thus *SME* (and its approximation, *AE*(12)) joins *Dst* as the magnetic indices with the most direct geophysical meaning. They are complementary in another manner: while *Dst* samples the ring current, composed of suprathermal magnetotail ions, *SME* samples the thermal portion of plasma sheet, specifically the electrons, which constitute the bulk of the precipitating energy. The two indices combine thus to sample both the thermal and suprathermal magnetospheric plasma populations.

[41] It has long been known from the study of individual substorms that when the auroral bulge does not pass over a contributing *AL*(12) station, that index does not reflect the onset. Therefore one might expect that the use of the SuperMAG derived *SML*, with typically more than 100 contributing magnetic stations, should considerably improve the detection of substorm onsets. A statistical study confirms this, documenting that *SML* can be used to identify a significantly larger number of onsets (about 30–40% more per year). Equally important is the fact that the *SML* onset times are much closer to the epochs inferred from global images (about a 4 min median time difference instead of 8 min). We used *SML* to produce a list of 10,719 substorms between 1 January 1997 and 31 December 2002; the list is intended to be comprehensive for this time interval, and is included as auxiliary material Data Set S1.[1] A superposed epoch analysis using DMSP data demonstrates that substorms, as defined by *SML*, correspond to a sharp and sustained rise in auroral power. For the case of isolated substorms, the rise in power and subsequent decline, which takes more than 2 h to complete, closely mirrors that produced from a list comprised from global imaging observations. However, the comprehensive nature of substorm modeling from *SML* suggests new possibilities. As a first example of the power of the *SML* database, we have demonstrated how recurrent substorms differ from isolated substorms. Among the specific differences are that for isolated substorms, broadband (wave) aurora rises much more sharply (about 186%) than any other type; whereas for recurrent substorms, all types of electron precipitation rise by roughly 60%. However, this difference can be attributed to the higher baseline for recurrent substorms. On an absolute basis, both recurrent and isolated substorms have about the same effect, to wit, raising the diffuse aurora by about 8 GW, and broadband aurora by about 1.5 GW.

[1]Auxiliary materials are available at ftp://ftp.agu.org/apend/journal/2011ja016779.

[42] **Acknowledgments.** This work was supported by NSF grants ATM-1132361 and ATM-1045638 to the Johns Hopkins University (P.T.N.) and by NASA grant NNX08AM32G (J.W.G.). The following PIs contributed data helping constitute the SME index: J. J. Love, I. Mann, K. Yumoto, K. Shiokawa, D. Boteler, S. McMillan, M. Moldwin, E. Tanskanen, C. Stolle, P. Chi, SPIDR/NOAA, O. Troshichev, M. Engebretson, UCLA/IGPP, Florida Institute of Technology, F. Honary, M. Conners, DTU Space, and IZMIRAN. Also, S.-I. Ohtani is the JHU/APL PI for SuperMAG, while K. Liou contributed the Polar UVI substorm list and auroral power data files.

References

Ahn, B.-H., H. W. Kroehl, Y. Kamide, and E. A. Kihn (2000), Universal time variations of the auroral electrojet indices, *J. Geophys. Res.*, *105*, 267–275, doi:10.1029/1999JA900364.

Ahn, B.-H., G.-H. Moon, W. Sun, S.-I. Akasofu, G. X. Chen, and Y. D. Park (2002), Universal time variation of the Dst index and the relationship between the cumulative AL and Dst indices during geomagnetic storms, *J. Geophys. Res.*, *107*(A11), 1409, doi:10.1029/2002JA009257.

Allen, J. H., and H. W. Kroehl (1975), Spatial and temporal distributions of magnetic effects of auroral electrojets as derived from *AE* indices, *J. Geophys. Res.*, *80*, 3667–3677, doi:10.1029/JA080i025p03667.

Chaston, C. C., J. W. Bonnell, C. W. Carlson, J. P. McFadden, R. E. Ergun, and R. J. Strangeway (2003), Properties of small-scale Alfvén waves and accelerated electrons from FAST, *J. Geophys. Res.*, *108*(A4), 8003, doi:10.1029/2002JA009420.

Chaston, C. C., J. W. Bonnell, C. W. Carlson, J. P. McFadden, R. E. Ergun, R. J. Strangeway, and E. J. Lund (2004), Auroral ion acceleration in dispersive Alfvén waves, *J. Geophys. Res.*, *109*, A04205, doi:10.1029/2003JA010053.

Chaston, C. C., C. W. Carlson, J. P. McFadden, R. E. Ergun, and R. J. Strangeway (2007), How important are dispersive Alfvén waves for auroral particle acceleration?, *Geophys. Res. Lett.*, *34*, L07101, doi:10.1029/2006GL029144.

Davis, T. N., and M. Sugiura (1966), Auroral electrojet activity index *AE* and its universal time variations, *J. Geophys. Res.*, *71*, 785–801.

Frey, H. U., S. B. Mende, V. Angelopoulos, and E. F. Donovan (2004), Substorm onset observations by IMAGE-FUV, *J. Geophys. Res.*, *109*, A10304, doi:10.1029/2004JA010607.

Gjerloev, J. W. (2009), A global ground-based magnetometer initiative, *Eos Trans. AGU*, *90*(27), 230, doi:10.1029/2009EO270002.

Gjerloev, J. W., R. A. Hoffman, M. M. Friel, L. A. Frank, and J. B. Sigwarth (2004), Substorm behavior of the auroral electrojet indices, *Ann. Geophys.*, *22*, 2135–2149, doi:10.5194/angeo-22-2135-2004.

Hoffman, R. A., and J. W. Gjerloev (2008), An automated procedure for determining quiet daily geomagnetic variations, *Eos Trans. AGU*, *89*(53), Fall Meet. Suppl., Abstract SM11B-1615.

Kamide, Y., and G. Rostoker (2004), What is the physical meaning of the AE index?, *Eos Trans. AGU*, *85*(19), 188, doi:10.1029/2004EO190010.

Kamide, Y., et al. (1982), Global distribution of ionospheric and field-aligned currents during substorms as determined from six IMS meridian chains of magnetometers: Initial results, *J. Geophys. Res.*, *87*, 8228–8240, doi:10.1029/JA087iA10p08228.

Liou, K., P. T. Newell, C.-I. Meng, A. T. Y. Lui, M. Brittnacher, and G. Parks (1997), Dayside auroral activity as a possible precursor of substorm onsets: A survey using Polar ultraviolet imagery, *J. Geophys. Res.*, *102*, 19,835–19,843, doi:10.1029/97JA01741.

Liou, K., P. T. Newell, D. G. Sibeck, C.-I. Meng, M. Brittnacher, and G. Parks (2001), Observation of IMF and seasonal effects in the location of auroral substorm onset, *J. Geophys. Res.*, *106*, 5799–5810, doi:10.1029/2000JA003001.

Mende, S. B., C. W. Carlson, H. U. Frey, L. M. Peicolas, and N. Ostgaard (2003), FAST and IMAGE-FUV observations of a substorm onset, *J. Geophys. Res.*, *108*(A9), 1344, doi:10.1029/2002JA009787.

Newell, P. T. (2000), Reconsidering the inverted-V particle signature: Relative frequency of large-scale electron acceleration events, *J. Geophys. Res.*, *105*, 15,779–15,794, doi:10.1029/1999JA000051.

Newell, P. T., T. Sotirelis, K. Liou, C.-I. Meng, and F. J. Rich (2007), A nearly universal solar wind-magnetosphere coupling function inferred from 10 magnetospheric state variables, *J. Geophys. Res.*, *112*, A01206, doi:10.1029/2006JA012015.

Newell, P. T., T. Sotirelis, and S. Wing (2009), Diffuse, monoenergetic, and broadband aurora: The global precipitation budget, *J. Geophys. Res.*, *114*, A09207, doi:10.1029/2009JA014326.

Newell, P. T., A. R. Lee, K. Liou, S.-I. Ohtani, T. Sotirelis, and S. Wing (2010), Substorm cycle dependence of various types of aurora, *J. Geophys. Res.*, *115*, A09226, doi:10.1029/2010JA015331.

Rostoker, G. (1972), Geomagnetic indices, *Rev. Geophys.*, *10*, 935–950, doi:10.1029/RG010i004p00935.

Stasiewicz, K., et al. (2000), Small scale Alfvénic structure in the aurora, *Space Sci. Rev.*, *92*, 423–533, doi:10.1023/A:1005207202143.

J. W. Gjerloev and P. T. Newell, Johns Hopkins University Applied Physics Laboratory, 11100 Johns Hopkins Rd., Laurel, MD 20723–6099, USA. (patrick.newell@jhuapl.edu)